DOR:

Research Paper

Nonlinear Buckling Analysis of Different Types of Porous FG Sandwich Beams with Temperature-Dependent

Mohsen Rahmani[1*], Younes Mohammadi[2], Mahdi Abtahi[2]
[1]Department of Mechanics, Tuyserkan Branch, Islamic Azad University, Tuyserkan, Iran
[2]Faculty of Industrial and Mechanical Engineering, Qazvin Branch, Islamic Azad University, Qazvin, Iran
[*]Email of the Corresponding Author: Mohsen_rahmani@ymail.com
Received: November 11, 2023; Accepted: January 6, 2024

Abstract
In this paper, the nonlinear buckling behavior of two types of functionally graded sandwich beams was studied using a high-order sandwich beam theory. Type I consists of functionally graded layers coating a homogeneous core, while type II features an FG core covered by homogeneous face sheets. All materials are considered temperature dependent, with FGM properties modified through even and uneven porosity distributions modeled by a power law rule. The sandwich beam theory was adjusted to account for nonlinear Lagrange strains, thermal stresses of the face sheets, in-plane strain, and the transverse flexibility of the core. The governing equations were derived from the minimum potential energy principle, and a Galerkin method was employed to solve them for simply supported and clamped boundary conditions. Comparisons with existing literature demonstrate good agreement. The resultes showed that critical load parameter decreases with increasing temperature, power law index, length-to-thickness ratio, thickness, and porosity volume fraction in both distributions, but increases with the wave number. Additionally, the stability of type II sandwich beams surpasses that of type I in high-temperature conditions.

Keywords
Porosity, FGM, Boundary Condition, High-order Sandwich Beam Theory

Symbols and Abbreviations

χ, ψ, z	Coordinate components	A	Stretching stiffness
h	Thickness(m)	B	bending-stretching stiffness
T	Temperature(K)	D	bending stiffness
C	coefficients of temperature	E	Young's modulus
δ	Variation	ν	Poisson's ratio
K	Kinetic Energy (J)	α	thermal expansion coefficient
U	Strain Energy (J)	N	Power law index
t,b,c	outer face-sheet, inner face-sheet and core index	n	Wave number
P	Every material properties	N	Stress Resultant
u, υ	In-plane deformation	M	Moment Resultant
w	Transverse deformation	$\hat{N}_x^j$	External in-plane loads
ζ	Porosity volume fraction	Cm	is the eigenvector

ce	Ceramic	λ	Lagrange multiplier
m	Metal	K	Stiffness matrix
σ	Normal stresses	G	geometric Matrix
ε	Normal strain		
τ	Shear stress		
γ	Shear strain		
ϕ	Rotation of the normal to the middle surface		

1. Introduction

To reach a high performance and high bending rigidity with a low weight, the concept of sandwich structures which are composed of two thin and stiff face sheets that cover a thick and soft core has been widely used in advanced industries such as nuclear reactors, aircraft, satellite and marine. In high-temperature environments, using ordinary composite materials and laminates in the sandwich panels leads to delamination, stress concentration, and failure. So, to eliminate these problems, functionally graded materials have been used which are inhomogeneous microscopic materials and their properties smoothly vary across the thickness. Since during the manufacturing of the FGMs, some microvoids, and porosities appeared that affect the materials properties, some porosity distributions have been proposed to modify the models of FGM in the analysis. Also, in high-temperature conditions, these properties are reduced. So it is important to consider the dependency of materials properties to the temperature [1, 2].

In classical theories, the core is considered as an inflexible layer, but it is a transversely flexible one, therefore, to accurate investigation of the mechanical behavior of sandwich structures, this effect should be considered. So, the high-order sandwich theory was presented [3]. Many researchers have studied the mechanical behaviors of sandwich beams such as buckling and post-buckling by using different theories. Based on a higher beam theory, Fazzolari surveyed the vibration and elastic stability of functionally graded sandwich beams resting on the elastic foundation [4]. Wu et al. surveyed the vibration and buckling of sandwich beams with FG carbon nanotube-reinforced composite faces based on the Timoshenko beam theory [5]. Li investigated the nonlinear vibration and stability of axially moving viscoelastic sandwich beams under resonances by using the Galerkin method [6]. Nguyen et al. studied the buckling and vibration behaviors of different types of FG sandwich beams by using a quasi-3D beam theory [7]. By using a finite element model, Kahya and Turan investigated the buckling and vibration of different types of FG sandwich beams based on the first-order shear deformation theory [8]. Tossapanon and Wattanasakulpong studied the buckling and vibration behavior of sandwich beams with FG faces resting on an elastic foundation based on the Timoshenko beam theory and Chebyshev collocation [9]. Nguyen et al. studied the vibration and buckling of FG sandwich beams based on the higher-order shear deformation theory [10]. Vo et al. studied the vibration and buckling of FG sandwich beams by using a quasi 3D theory and a finite element model [11]. Challamel and Girhammar studied the buckling of partial composite beam-columns based on the variational theories and by considering the shear and axial effects [12]. Bhangale and Ganesan investigated the thermoelastic buckling and vibration behavior of FG sandwich beams with viscoelastic core by using a finite element formulation [13]. Based on a unified higher-order shear deformation beam theory, Hamed et al. studied the buckling behavior of sandwich

composite laminated beams resting on elastic foundations by considering the effect of in-plane varying compressive force [14]. Li et al. studied the thermal post-buckling of sandwich beams with functionally graded negative Poisson's ratio honeycomb core by using 3D full-scale finite element simulations [15]. Liu et al. studied the thermal-mechanical coupling buckling analysis of porous FG sandwich beams based on the high-order sinusoidal shear deformation theory [16]. Paul and Das investigated the nonlinear post-buckling load of tapered functionally graded material beams based on Timoshenko beam theory [17]. Yin et al. studied the bending and free vibration responses of composite laminated and sandwich beams, Based on the two-dimensional elastic theory [18]. Askari et al. studied the vibration of coupled transverse and shear piezoelectric FG porous beams by using higher-order theories [19]. Fouda et al. investigated the bending, buckling and vibration of FG porous beam based on a finite element model [20]. Gao et al. analyzed the buckling behaviors of the FG cylindrical beams with radially and axially varying material in-homogeneities by a high-order cylindrical beam model [21]. Basaglia and Camotim studied the buckling behavior of thin-walled steel structural systems by using the application of beam finite element models based on generalized beam theory for different support conditions and subjected to various loadings [22]. Akbas studied the post-buckling analysis of an edge-cracked cantilever beam composed of functionally graded material (FGM) subjected to axial compressive loads by using the total Lagrangian Timoshenko beam element approximation [23]. Grygorowicz et al. dealt with elastic buckling of sandwich beam with metal foam both analytically and numerically [24]. Ellahi et al. studied thermal buckling behavior of FG beams attached with piezoelectric layers based on third order shear deformation beam theory [25]. Nejati et al. discussed about buckling and vibration behavior of SMA hybrid composite sandwich beams with FG core under thermal condition based on higher order theory [26]. Chai et al. investigated a method for suppressing nonlinear flutter and thermal buckling of composite lattice sandwich beams based on the von Kármán large-deflection theory [27]. Safaei et al. studied buckling and bending behavior of carbon foam sandwich beams under a thermal load and axial compression [28]. Mesmoudi et al. studied an approach to nalyze the nonlinear bending and buckling behavior of FG sandwich beams [29]. Eltaher and Mohamed investigated the buckling stability of sandwich laminated composite beams under the compression of axial load based on higher shear deformation theory [30]. Liu et al. studied the buckling behavior of FG sandwich beams based on the scaled boundary finite element method [31]. Belarbi et al. investigated the buckling behavior of FG curved sandwich beams based on a refined shear theory. This theory has three unknowns [32]. Waddar et al. studied the buckling and vibration behavior of sandwich beams with composite facing and syntactic foam based on the experimental load-deflection data and performing experimental modal analysis [33].

In the present research, for the first time, the nonlinear buckling behavior of two types of sandwich beams is studied based on a modified high-order sandwich beam theory. In type I, the sandwich beam composes two functionally graded material face sheets and a homogeneous core, and in type II, two homogeneous face sheets coat a functionally graded core. Even and uneven porosity distributions are considered within the power law rule to model the FGMs. All material properties are temperature dependent and the temperature distribution is uniform. To increase the accuracy of the analysis, in-plane stresses and high order stresses of the core, and thermal stresses and thermal stress resultants of the face-sheets and core are considered concurrently, which are ignored in many of the references.

The equations are derived based on the minimum potential energy principle. In this model, Lagrange strains are used which takes into account the nonlinear term neglected in several works of the literature. By considering this term more accurate answers have been obtained. A Galerkin method is used to solve the equations for clamped and simply supported boundary conditions. The effects of the temperature variation, some geometrical parameters, and porosity variation on the critical load of sandwich beams are investigated, too.

2. Formulation

A schematic cross-section of different types of sandwich beams is shown in Figure 1. In sandwich type-I, a homogeneous core is covered by two porous FG face sheets, and in sandwich type-II the homogeneous face sheets cover a porous FG core.

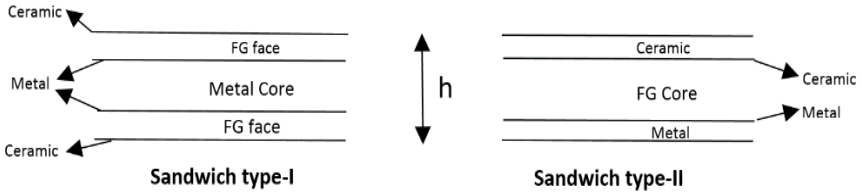

Figure 1. A schematic of various models of sandwich beams

Homogeneous materials and the FGMs have temperature-dependent properties, which are modeled as follows [34]:

$$P = P_0\left(P_{-1}T^{-1} + 1 + P_1T + P_2T^2 + P_3T^3\right) \tag{1}$$

Files Where "P"s are coefficients of temperature, and they are unique for each material; $T=T_0+\Delta T$, which T_0 is equal to 300(K). A power law rule which is modified by considering the porosity volume fraction is applied to model the FGM properties. The power law rule which consists of even porosity distribution is presented for type I as follows [24]:

$$P_j\left(z_j,T\right) = g\left(z_j\right)P_{ce}^j\left(T\right) + \left[1 - g\left(z_j\right)\right]P_m^j\left(T\right) - \left(P_{ce}^j\left(T\right) + P_m^j\left(T\right)\right)\frac{\zeta}{2} \tag{2}$$

$$g\left(z_t\right) = \left(\frac{\frac{h_t}{2} - z_t}{h_t}\right)^N;\quad g\left(z_b\right) = \left(\frac{\frac{h_b}{2} + z_b}{h_b}\right)^N;\quad j = (t,b) \tag{3}$$

And for sandwich-type II is as follows [34]:

$$P_c\left(z_c,T\right) = g\left(z_c\right)P_{ce}^c\left(T\right) + \left[1 - g\left(z_c\right)\right]P_m^c\left(T\right) - \left(P_{ce}^c\left(T\right) + P_m^c\left(T\right)\right)\frac{\zeta}{2} \tag{4}$$

$$g\left(z_c\right) = \left(\frac{\frac{h_c}{2} - z_c}{h_c}\right)^N \tag{5}$$

where "N" is the constant power law index; g(z) and [1-g(z)] are volume fractions of ceramic and metal; "ζ" is the porosity distribution; and subscripts "t", "b" and "c" refer to top and bottom faces and the core, respectively; “h” is thickness and “P” is the material properties such as elastic moduli,

density, Poisson's ratio, and thermal expansion coefficient. In the uneven case, the micro voids are spread in the middle area of the layers decrease near the edges, and tend to the zero. So, the power law rule in the uneven case for the type-I is modified as follows [34]:

$$P_j\left(z_j,T\right)=g\left(z_j\right)P_{ce}^{j}\left(T\right)+\left[\,1-g\left(z_j\right)\right]P_m^j\left(T\right)-\left(P_{ce}^{j}\left(T\right)+P_m^j\left(T\right)\right)\frac{\zeta}{2}\left(1-\frac{2\left|z_j\right|}{h}\right),(j=t,b) \quad (6)$$

In the type-II, it is presented as follows [34]:

$$P_c\left(z_c,T\right)=g\left(z_c\right)P_{ce}^{c}\left(T\right)+\left[\,1-g\left(z_c\right)\right]P_m^c\left(T\right)-\left(P_{ce}^{c}\left(T\right)+P_m^c\left(T\right)\right)\frac{\zeta}{2}\left(1-\frac{2\left|z_c\right|}{h}\right) \quad (7)$$

The minimum potential energy principle is used to obtain the governing equations of sandwich beams which include the potential of the external loads, "V", and total strain energy, "U"; This principle is presented as follows [35]:

$$\prod(\delta U+\delta V)=0 \quad (8)$$

which "δ" denotes the variation operator. The variation of the total strain energy includes mechanical stresses with linear and thermal stresses with nonlinear strains in the faces and core. The compatibility conditions rule as constraints which are attended as four Lagrange multipliers in the principle. By considering the in-plane stresses of the core, "δU" is as follows:

$$\begin{aligned}
&\delta U_p=\int_{A_t}\left(\sigma_{xx}^{t}\delta\varepsilon_{xx}^{t}+\sigma_{xx}^{tT}\delta d_{xx}^{t}+\tau_{xz}^{t}\delta\gamma_{xz}^{t}+\sigma_{zz}^{tT}\delta d_{zz}^{t}\right)dA+\\
&\int_{A_b}\left(\sigma_{xx}^{b}\delta\varepsilon_{xx}^{b}+\sigma_{xx}^{bT}\delta d_{xx}^{b}+\tau_{xz}^{b}\delta\gamma_{xz}^{b}+\sigma_{zz}^{bT}\delta d_{zz}^{b}\right)dv+\\
&\int_{A_{core}}\left(\sigma_{xx}^{c}\delta\varepsilon_{xx}^{c}+\sigma_{xx}^{cT}\delta d_{xx}^{c}+\sigma_{zz}^{c}\delta\varepsilon_{zz}^{c}+\sigma_{zz}^{cT}\delta d_{zz}^{c}+\tau_{xz}^{c}\delta\gamma_{xz}^{c}\right)dv+\\
&\delta\int_{0}^{L}\left[\lambda_{xt}\left(u_t\left(z_t=\frac{h_t}{2}\right)-u_c\left(z_c=-\frac{h_c}{2}\right)\right)+\lambda_{zt}\left(w_t-w_c\left(z_c=-\frac{h_c}{2}\right)\right)+\right.\\
&\left.\lambda_{xb}\left(u_c\left(z_c=\frac{h_c}{2}\right)-u_b\left(z_b=-\frac{h_b}{2}\right)+\lambda_{zb}\left(w_c\left(z_c=\frac{h_c}{2}\right)-w_b\right)\right]dx
\end{aligned} \quad (9)$$

where "σ_{xx}" is the in-plane normal stress; "τ_{xz}" is the in-plane shear stresses; "ε_{xx}" and "γ_{xz}" display the in-plane normal and shear linear strains; "dxx" and "d_{zz}" are the nonlinear in-plane normal and shear strains of the layers; "σ^{T}_{xx}" and "σ^{T}_{zz}" express the thermal stresses; "σ_{zz}" and "ε_{zz}" present the lateral normal stress and strain; and "λ_x" and "λ_z" are the Lagrange multipliers. It should be noted that the material properties in the functionally graded layers are the function of the displacement and the temperature, and in the homogeneous layers are just a function of the temperature. The variation of the external loads is as follows:

$$\delta V=-\int_0^L\left(P_t\delta w_0^t+P_b\delta w_0^b+n_x^t\delta u_0^t+n_x^b\delta u_0^b\right)dx \quad (10)$$

where "u_0^j" and w_0^j (j = t, b) are the displacements of the mid-plane of the face sheets in the longitudinal and vertical directions, respectively; "n_x^j" (j=t, b) are the in-plane external loads of the top and bottom face sheets; and, "P_t" and "P_b" are the vertical distributed loads applied on the top and bottom face sheets, respectively. The displacement fields of the face sheets are modeled by the first-order shear deformation theory.

$$u_j\left(x,z,t\right)=u_{0j}\left(x,t\right)+z_j\phi_{xj}\ j=(t,b) \tag{11}$$

$$w_j\left(x,z,t\right)=w_{0j}\left(x,t\right) \tag{12}$$

where subscript "0" expresses values in association with the middle surface of the layers; and "ϕ" is the rotation of the normal to the middle surface. The kinematic relations of the core are presented as cubic patterns which contain seven unknown coefficients as follows [36]:

$$u_c\left(x,z_c,t\right)=u_0\left(x,t\right)+u_1\left(x,t\right)z_c+u_2\left(x,t\right)z_c^2+u_3\left(x,t\right)z_c^3 \tag{13}$$

$$w_c\left(x,z_c,t\right)=w_0\left(x,t\right)+w_1\left(x,t\right)z_c+w_2\left(x,t\right)z_c^2 \tag{14}$$

The strain components of the layers are presented by the Lagrange strain tensor as follows [36]:

$$\varepsilon_{xx}^j=u_{j,x}+\frac{1}{2}\left(w_{0j,x}\right)^2-\alpha_j\Delta T_j,\ j=\left(t,b\right) \tag{15}$$

$$\varepsilon_{zz}^j=\frac{1}{2}\phi_{jx}^2-\alpha_j\Delta T_j \tag{16}$$

$$\gamma_{xz}^j\left(x,z_j,t\right)=u_{j,z}(x,t)+w_{j,x}(x,t)+u_{j,x}(x,t)u_{j,z}(x,t)+w_{j,x}(x,t)w_{j,z}(x,t) \tag{17}$$

The"(), i" expresses derivation for "i". The strain of the core can be defined as:

$$\varepsilon_{xx}^c\left(x,z_c,t\right)=u_{c,x}\left(x,z_c,t\right)+\frac{1}{2}\left(w_{0c,x}\right)^2-\alpha_c\Delta T \tag{18}$$

$$\varepsilon_{zz}^c\left(x,z_c,t\right)=w_{c,z}\left(x,z_c,t\right)+\frac{1}{2}\left(\phi_{0c}\right)^2+\frac{1}{2}\left(w_{1c}\right)^2-\alpha_c\Delta T \tag{19}$$

$$\gamma_{xz}^c\left(x,z_c,t\right)=u_{c,z}(x,z_c,t)+w_{c,x}(x,z_c,t)+\phi_{0c}u_{0c,x}+w_{1c}w_{0c,x} \tag{20}$$

With algebraic operations by substituting the displacement components and by using the compatibility conditions in Equations (9) and (10), thirteen equations are derived:

$$u_{0t}+\frac{h_t}{2}\phi^t=u_{0c}-\frac{h_c}{2}\phi_0^c+\frac{h_c^2}{4}u_{2c}-\frac{h_c^3}{8}u_{3c} \tag{21}$$

$$w_{0t}=+w_{0c}-\frac{h_c}{2}w_{1c}+\frac{h_c^2}{4}w_{2c} \tag{22}$$

$$u_{0b}-\frac{h_b}{2}\phi^b=u_{0c}+\frac{h_c}{2}\phi_0^c+\frac{h_c^2}{4}u_{2c}+\frac{h_c^3}{8}u_{3c} \tag{23}$$

$$w_{0b}=+w_{0c}+\frac{h_c}{2}w_{1c}+\frac{h_c^2}{4}w_{2c} \tag{24}$$

Based on the Equations (21-24) the displacements of the face-sheets are dependent on the core, so the unknown decreases to nine and the number of the governing equations is nine.

$$+\frac{h_t}{2}N_{x,x}^t-M_{x,x}^t+N_z^{tT}\phi_x^t+N_{xz}^t+\frac{h_t}{2}n_x^t=0 \tag{25}$$

$$-\frac{h_b}{2}N^b_{x,x}-M^b_{x,x}+N^{bT}_z\phi^b_x+N^b_{xz}-\frac{h_b}{2}n^b_x=0 \tag{26}$$

$$-N^t_{x,x}-N^b_{x,x}-N^c_{x,x}-n^t_x-n^b_x=0 \tag{27}$$

$$+\frac{h_c}{2}N^t_{x,x}-\frac{h_c}{2}N^b_{x,x}-M^c_{1,x}+N^{cT}_z\phi^c_0+N^c_{xz}+\frac{h_c}{2}n^t_x-\frac{h_c}{2}n^b_x=0 \tag{28}$$

$$-\frac{h_c^2}{4}N^t_{x,x}-\frac{h_c^2}{4}N^b_{x,x}-M^c_{2,x}+2M^c_{xz1}-\frac{h_c^2}{4}n^t_x-\frac{h_c^2}{4}n^b_x=0 \tag{29}$$

$$+\frac{h_c^3}{8}N^t_{x,x}-\frac{h_c^3}{8}N^b_{x,x}-M^c_{3,x}+3M^c_{xz2}+\frac{h_c^3}{8}n^t_x-\frac{h_c^3}{8}n^b_x=0 \tag{30}$$

$$\begin{aligned}&-N^t_x(w^c_0)+\frac{h_c}{2}N^t_x(w^c_1)-\frac{h_c^2}{4}N^t_x(w^c_2)-N^{tT}_{x,x}w^c_{0,x}-N^{tT}_x w^c_{0,xx}+\frac{h_c}{2}N^{tT}_{x,x}w^c_{1,x}+\frac{h_c}{2}N^{tT}_{x,x}w^c_{1,x}-\\&\frac{h_c^2}{4}N^{tT}_{x,x}w^c_{2,x}-\frac{h_c^2}{4}N^{tT}_x w^c_{2,xx}-N^t_{xz,x}-N^b_x(w^c_0)-\frac{h_c}{2}N^b_x(w^c_1)-\frac{h_c^2}{4}N^b_x(w^c_2)-N^{bT}_{x,x}w^c_{0,x}-N^{bT}_x w^c_{0,xx}\\&-\frac{h_c}{2}N^{bT}_{x,x}w^c_{1,x}-\frac{h_c}{2}N^{bT}_{x,x}w^c_{1,x}-\frac{h_c^2}{4}N^{bT}_{x,x}w^c_{2,x}-\frac{h_c^2}{4}N^{bT}_x w^c_{2,xx}-N^b_{xz,x}-N^c_{xz,x}-\widehat{N^c_x(w^c_0)}-N^{cT}_{x,x}w^c_{0,x}\\&-N^{cT}_x w^c_{0,xx}-P_t-P_b=0\end{aligned} \tag{31}$$

$$\begin{aligned}&+\frac{h_c}{2}N^t_x(w^c_0)-\frac{h_c^2}{4}N^t_x(w^c_1)+\frac{h_c^3}{8}N^t_x(w^c_2)+\frac{h_c}{2}N^{tT}_{x,x}w^c_{0,x}+\frac{h_c}{2}N^{tT}_x w^c_{0,xx}-\frac{h_c^2}{4}N^{tT}_{x,x}w^c_{1,x}\\&-\frac{h_c^2}{4}N^{tT}_{x,x}w^c_{1,xx}+\frac{h_c^3}{8}N^{tT}_{x,x}w^c_{2,x}+\frac{h_c^3}{8}N^{tT}_x w^c_{2,xx}+\frac{h_c}{2}N^t_{xz,x}-\frac{h_c}{2}N^b_x(w^c_0)-\frac{h_c^2}{4}N^b_x(w^c_1)-\\&\frac{h_c^3}{8}N^b_x(w^c_2)-\frac{h_c}{2}N^{bT}_{x,x}w^c_{0,x}-\frac{h_c}{2}N^{bT}_x w^c_{0,xx}-\frac{h_c^2}{4}N^{bT}_{x,x}w^c_{1,x}-\frac{h_c^2}{4}N^{bT}_{x,x}w^c_{1,xx}-\frac{h_c^3}{8}N^{bT}_{x,x}w^c_{2,x}\\&-\frac{h_c^3}{8}N^{bT}_x w^c_{2,xx}-\frac{h_c}{2}N^b_{xz,x}+N^c_z+N^c_z+N^{cT}_z w^c_1-M^c_{xz1,x}+\frac{h_c}{2}P_t-\frac{h_c}{2}P_b=0\end{aligned} \tag{32}$$

$$\begin{aligned}&-\frac{h_c^2}{4}N^t_x(w^c_0)+\frac{h_c^3}{8}N^t_x(w^c_1)-\frac{h_c^4}{16}N^t_x(w^c_2)-\frac{h_c^2}{4}N^{tT}_{x,x}w^c_{0,x}-\frac{h_c^2}{4}N^{tT}_x w^c_{0,xx}+\frac{h_c^3}{8}N^{tT}_{x,x}w^c_{1,x}\\&+\frac{h_c^3}{8}N^{tT}_{x,x}w^c_{1,x}-\frac{h_c^4}{16}N^{tT}_{x,x}w^c_{2,x}-\frac{h_c^4}{16}N^{tT}_x w^c_{2,xx}-\frac{h_c^2}{4}N^t_{xz,x}-\frac{h_c^2}{4}N^b_x(w^c_0)-\frac{h_c^3}{8}N^b_x(w^c_1)-\\&\frac{h_c^4}{16}N^b_x(w^c_2)-\frac{h_c^2}{4}N^{bT}_{x,x}w^c_{0,x}-\frac{h_c^2}{4}N^{bT}_x w^c_{0,xx}-\frac{h_c^3}{8}N^{bT}_{x,x}w^c_{1,x}-\frac{h_c^3}{8}N^{bT}_{x,x}w^c_{1,x}-\frac{h_c^4}{16}N^{bT}_{x,x}w^c_{2,x}-\\&\frac{h_c^4}{16}N^{bT}_x w^c_{2,xx}-\frac{h_c^2}{4}N^b_{xz,x}+2M^c_z-M^c_{xz2,x}-\frac{h_c^2}{4}P_t-\frac{h_c^2}{4}P_b=0\end{aligned} \tag{33}$$

In the relations of the face sheets, the "N"s depict the in-plane stress resultants; "M"s refer to the moment resultants; and "Nxz"s display the out-of-plane shear stress resultants, respectively, which are calculated as follows [36] :

$$N^j_{xx}=A_{11}u^j_{0,x}+B_{11}\phi^j_{,x}-N^{jT}_{xx},\ j=(t,b) \tag{34}$$

$$M^j_{xx}=B_{11}u^j_{0,x}+D_{11}\phi^j_{,x}-M^{jT}_{xx} \tag{35}$$

$$N^j_{xz}=\pi^2/_{12}A_{44}(\phi^j+w^j_{0,x}) \tag{36}$$

“A” is the stretching stiffness; “B” is the bending-stretching stiffness; and “D” is the bending stiffness; which are constant coefficients and expressed as:

$$\begin{Bmatrix} A_{11}^{j} \\ B_{11}^{j} \\ D_{11}^{j} \end{Bmatrix} = \int_{-hj/2}^{hj/2} \left(\frac{E_j}{1-\nu_j{}^2} \right) \begin{Bmatrix} 1 \\ z_j \\ z_j^2 \end{Bmatrix} dz_j \qquad (37)$$

$$\left\{ A_{44}^{j} \right\} = \int_{-hj/2}^{hj/2} \left(\frac{E_j}{1+2\nu_j} \right) dz_j$$

"N^T" and "M^T" display the high-order thermal stress and momentum resultants in the face sheets which are depicted as follows:

$$\begin{Bmatrix} N_{xx}^{jT}, N_{zz}^{jT} \\ M_{xx}^{jT} \end{Bmatrix} = -\int_{-hj/2}^{hj/2} \left(\frac{E_j}{1-\nu_j} \alpha_j . T_j \right) \begin{Bmatrix} 1 \\ z_j \end{Bmatrix} dz_j \ , j=(t,b,c) \qquad (38)$$

Where "E", "ν" and "α" are Young's modulus, the Poisson's ratio, and the thermal expansion coefficient, respectively, which in the functionally graded layers are the function of the displacement, too. The high-order stress resultants of the core are as follows:

$$N_{xzc}, M_{xz1}, M_{xz2} = \int_{-hc/2}^{hc/2} \left(1, z_c, z_c^2\right) \tau_{xz}^{c} dz_c \qquad (39)$$

$$N_{zc}, M_{zc} = \int_{-hc/2}^{hc/2} \left(1, z_c\right) \sigma_{zz}^{c} dz_c \qquad (40)$$

$$N_x^c, M_1^c, M_2^c, M_3^c = \int_{-hc/2}^{hc/2} \left(1, z_c, z_c^2, z_c^3\right) \sigma_{xx}^{c} dz_c \qquad (41)$$

Finally, by substituting the high-order stress resultants in terms of the kinematic relations, the equations are derived in terms of the nine unknowns. On the other hand, $N_x^j(w_l^c)$ is defined as follows [37]:

$$N_x^j(w_l^c) = N_{x,x}^j w_{l,x}^c + N_x^j w_{l,xx}^c \ ; j=(t,b,c), l=(0,1,2) \qquad (42)$$

Where $\hat{N}_x^j$ are the external in-plane loads exerted to the top and bottom face sheets and the core, which are the parts of the total external load, $\hat{N}_0$, as follows:

$$N_x^t + N_x^b + N_x^c = -N_0 \qquad (43)$$

In this analysis, a uniform state of strain for the face sheets and the core is assumed. At edges 'x=0" or "x=L" and with a little simplification the equilibrium equations can be defined as:

$$\frac{N_x^t}{h_t \bar{E}_t} = \frac{N_x^b}{h_b \bar{E}_b} = \frac{N_x^c}{h_c \bar{E}_c} \qquad (44)$$

Where $\bar{E}_j$ is the equilibrium elasticity modulus of the layers that are defined as:

$$\bar{E}_j = \frac{\int_{-h_j/2}^{h_j/2} E_j\left(z_j\right) dz_j}{h_j} ; j=(t,b,c) \tag{45}$$

Hence, by using Equations (44) and (45), the external in-plane loads exerted on the face sheets and the core along the "x" direction can be obtained as:

$$\begin{Bmatrix} N_x^t \\ N_x^b \\ N_x^c \end{Bmatrix} = \frac{-N_0}{h_t\bar{E}_t + h_b\bar{E}_b + h_c\bar{E}_c} \begin{Bmatrix} h_t\bar{E}_t \\ h_b\bar{E}_b \\ h_c\bar{E}_c \end{Bmatrix} \tag{46}$$

3. Numerical Results

A Galerkin procedure is applied to solve the governing equations of two types of FG sandwich beams, with nine trigonometric shape functions, which satisfy the boundary conditions. The shape functions of simply supported boundary conditions are expressed as follows:

$$\phi_j = \left\lfloor C_{\phi j} \cos a_m x \right\rfloor e^{i\omega t} \quad , j=(t,b,c) \tag{47}$$

$$u_{ck} = \left\lfloor C_{uck} \cos a_m x \right\rfloor e^{i\omega t} \qquad k=(0,1,2) \tag{48}$$

$$w_l = \left\lfloor C_{wl} \sin a_m x \right\rfloor e^{i\omega t} \qquad l=(0,1,2) \tag{49}$$

The shape functions of the clamped boundary condition [37] can be expressed as:

$$\phi_j = \left\lfloor C_{\phi j} \cos a_m x \right\rfloor e^{i\omega t} \quad , j=(t,b,c) \tag{50}$$

$$u_{ck} = \left\lfloor C_{uck} \sin a_m x \right\rfloor e^{i\omega t} \qquad k=(0,1,2) \tag{51}$$

$$w_l = C_{wl}\left(\sinh\left(\frac{\lambda_m x}{L}\right) - \sin\left(\frac{\lambda_m x}{L}\right) + \gamma_m\left(\cos h\left(\frac{\lambda_m x}{L}\right) - \cos\left(\frac{\lambda_m x}{L}\right)\right)\right)e^{i\omega t} \tag{52}$$

$$\cos\lambda_m . \cosh\lambda_m = 1 \tag{53}$$

$$\gamma_m = \frac{\sinh\lambda_m - \sin\lambda_m}{\cos\lambda_m - \cosh\lambda_m} \quad m=(1,2,3,\ldots) \tag{54}$$

Where "$a_m = m\pi/L$"; "m" is the wave number and "C_{uk}, C_{wk}, C_{ϕ_j}" are the nine unknown constants of the shape functions. These nine equations can be displayed with a 9×9 matrix as follows:

$$(k_m - N_0 \times G_m)C_m = 0 \tag{55}$$

C_m is the eigenvector which contains nine unknown constants; "G" is the geometric and "K" is the stiffness matrices. To validate the results of the present approach, they are compared with the results of literature [11, 39], which are shown in Table 1 and Table 2, for the simply supported (S-S) and

clamped (C-C) boundary conditions. It's seen that there are good agreements between the present results and the literature.

Table 1. Critical load parameters of present results and literatures [11, 29] for (S-S).

N	Theory	2-1-2	1-1-1	1-8-1
	L/h=5			
0	Vo et al. (HOBT) [39]	48.5959	48.5959	48.5959
	Vo et al. (quasi-3D) [11]	49.5906	49.5906	49.5906
	Present	50.7611	50.7611	50.7611
1	Vo et al. (HOBT) [39]	22.2108	24.5596	38.7838
	Vo et al. (quasi-3D) [11]	22.7065	25.1075	39.6144
	Present	23.0681	25.1621	39.8011
	L/h=20			
0	Vo et al. (HOBT) [39]	53.2364	53.2364	53.2364
	Vo et al. (quasi-3D) [11]	53.3145	53.3145	53.3145
	Present	55.7922	55.7922	55.7922
1	Vo et al. (HOBT) [39]	23.4211	25.9588	41.9004
	Vo et al. (quasi-3D)	23.4572	25.9989	41.9639
	Present	23.5221	26.0847	41.0498

Table 2: Critical load parameters of present results and literature [11, 29] for (C-C).

N	Theory	2-1-2	1-1-1	1-8-1
	L/h=5			
	Vo et al. (HOBT) [39]	152.1470	152.1470	152.1470
0	Vo et al. (quasi-3D) [11]	160.2780	160.2780	160.2780
	Present	162.3531	162.3531	162.3531
	Vo et al. (HOBT) [39]	80.1670	83.8177	125.3860
1	Vo et al. (quasi-3D) [11]	85.2092	89.0834	132.5510
	Present	86.3562	90.9678	136.2631
	L/h=20			
	Vo et al. (HOBT) [39]	208.9510	208.9510	208.9510
0	Vo et al. (quasi-3D) [11]	210.7420	210.7420	210.7420
	Present	205.9696	205.9696	205.9696
	Vo et al. (HOBT) [39]	92.6741	102.6650	164.9490
1	Vo et al. (quasi-3D) [11]	93.5248	103.6060	166.4060
	Present	93.6145	102.9041	165.6243

Consider different types of FG sandwich beams which are assumed to be made from a mixture of Silicon nitride as ceramic phases and Stainless steel as metal phases. The temperature-dependent properties of constituent materials which are introduced by Equation (1) are available in reference [40]. In general, the "h_t-h_c-h_b" sandwich beam is a structure with the indices of top face sheet thickness, core thickness, and bottom face sheet thickness equal to "h_t", "h_c" and "h_b", respectively. Therefore, in a 1-8-1 sandwich, the thickness of the core is eight times each face sheet thickness. For simplicity, the non-dimensional critical load parameter is defined as follows:

$$N_{cr} = \frac{N_o}{10^9} \tag{56}$$

The material properties of structures are affected in high-temperature conditions. Based on equation (1), increasing the temperature reduces the Young modulus and density of metal and ceramic. As a result, the strength of the panels is reduced, which is an important reason for decreasing the critical load in high-temperature conditions. Figure 2 shows the critical parameter variation versus the temperature for two types of 1-8-1 FG sandwich beams with simply supported (S-S) and clamped (C-C) boundary conditions. Geometrical parameters are "h=0.02m, L/h=5, m=1". By increasing the temperature, the critical load parameters decrease. As shown in Figure 2, when N=0, the FG layers are made of full ceramic, as a result, the stability and resistance against the high-temperature conditions are more than the other values of "N", so critical load parameters are higher than others. By increasing the power law index, "N", the amount of ceramic reduces in the structure which causes the young modulus of the FGM and the stability of the structures to decrease. In a 1-8-1 sandwich, the core thickness is eight times the face sheet, so in sandwich type II which has an FG core, the amount of the ceramic is more than the type I. As a result, the stability and resistance of type II are higher than that of type I, so the critical load parameter of type II is higher. When N=2, in sandwiches type-I and type-II, with simply supported boundary condition (S-S), the amount of the ceramic is low in the FG layers, so, in the high temperature the stability of the structure is very low. The critical load parameters of the sandwiches with simply supported boundary conditions are lower than sandwiches with clamped (C-C) boundary conditions. Based on the Figure 2, the sandwich type-II with the clamped boundary condition is most resistant sandwich in the high temperature environments. The sandwich type-II is proper than the type-I in the same boundary condition for using in the thermal conditions. Also, in sandwich type-I (S-S), when "N=0", by increasing the temperature, the critical load parameter decreases 85.00%, for "N=1" and "N=2" it decreases 97.77%, and 97.44%, respectively. In sandwich type-I (C-C), when "N=0", by increasing the temperature, the critical load parameter decreases 60.51%, for "N=1" and "N=2" it decreases 68.03%, and 70.49%, respectively. And in sandwich type-II (S-S), when "N=0", by increasing the temperature, the critical load parameter decreases 90.10%, for "N=1" and "N=2" it decreases 81.15%, and 77.53%, respectively. And in sandwich type-II (C-C), when "N=0", by increasing the temperature, the critical load parameter decreases 33.03%, for "N=1" and "N=2" it decreases 49.78%, and 55.00%, respectively.

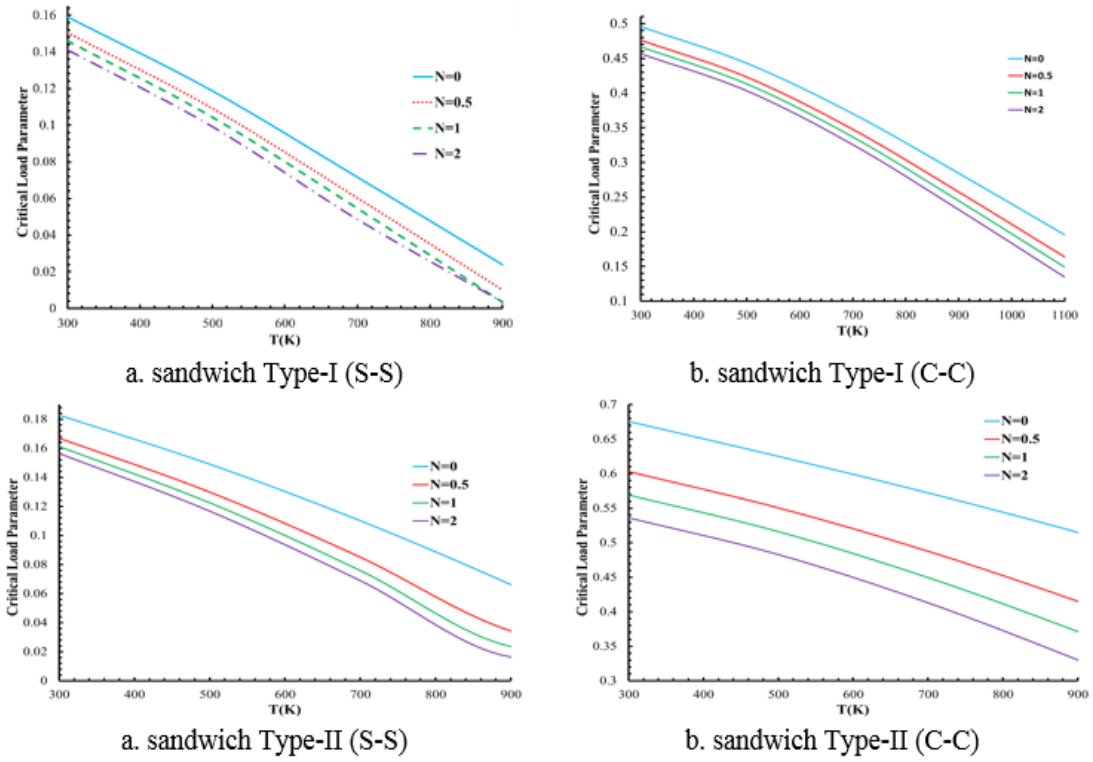

Figure 2. Critical load variation versus temperature in different types of sandwich beams

Figure 3 shows the effect of the length-to-thickness ratio (L/h) on the critical load parameter for 1-8-1 FG sandwich beams in the simply supported (S-S) and clamped (C-C) boundary conditions. Geometrical parameters are "h = 0.02m, T=300K, m=1". When ratios are increased in a constant "N", the critical load parameter decreases in all boundary conditions. The slope of decreasing the critical load parameter of the (S-S) sandwiches for both types is more than the (C-C) ones which shows the boundary condition has an impressive effect on the stability. In both types of sandwiches, the critical load parameter of (S-S) boundary conditions, is too lower than (C-C) ones. It has been shown that in the same boundary condition, the critical load parameters of sandwich-type I are lower than sandwich-type II. Since the thicknesses of the FG layers in sandwich type-II are higher than the sandwich type-I, increasing the power law index, N, has more effect on type-II. Based on Figure 3, by increasing this ratio, the stability of the structure is reduced and it is important to consider that long length is not proper for the FG sandwich beams. Also, it is obvious that, by increasing the power law index, "N", the critical load parameters decrease, but in this case effect of variation of the length is a dominant parameter and its variation has an impressive effect on the stability. For example, in sandwich type-I (S-S), for "L/h=5", by increasing "N", the critical load parameter decreased 11.29%, but for "N=0", by increasing this ratio, the critical load parameter decreased 96.87%. In sandwich type-I (C-C), for "L/h=5", by increasing "N", the critical load parameter decreases 7.86%, but for "N=0", by increasing this ratio, the critical load parameter decreases 24.34%. In sandwich type-II (S-S), for "L/h=5", by increasing "N", the critical load parameter decreases 14.41%, but for "N=0", by increasing this ratio, the critical load decreases 96.96%. And, in sandwich type-II (C-C), for "L/h=5", by increasing "N", the critical load parameter decreases by 20.66%, but for "N=0", by increasing this ratio, the critical

load decreases by 20.59%. Also, it should be noted that when the ratio is more than 12, the slope of the variation of the critical load decreases significantly.

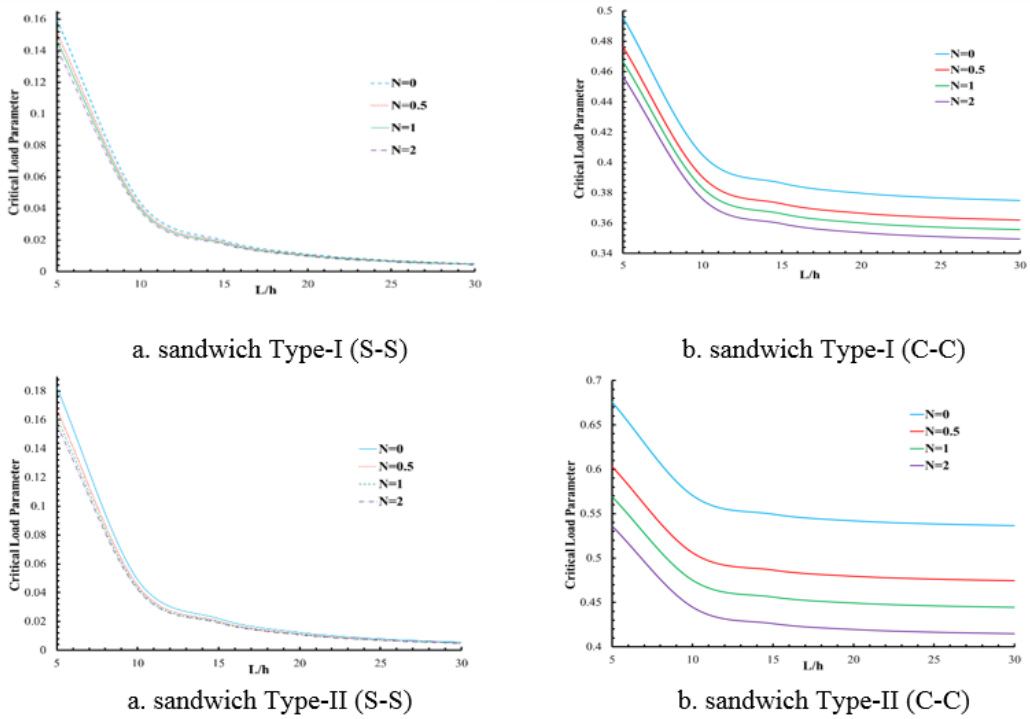

a. sandwich Type-I (S-S) b. sandwich Type-I (C-C)

a. sandwich Type-II (S-S) b. sandwich Type-II (C-C)

Figure 3. Critical load variation versus L/h ratio in different types of sandwich beams

Figure 4 shows the variation of the core-to-face sheet thickness ratio, “hc/ht”, on the critical load parameter in various power law indices and a constant total thickness. Geometrical parameters are “h=0.02m, T=300K, m=1, L/h=10”. When “hc/ht=0.5”, it means the face sheets' thicknesses are two times the core thickness, so it shows the results of the 2-1-2 sandwich. And, when “hc/ht=8”, it shows the results of the 1-8-1 sandwich. In sandwich type I and 2-1-2 sandwiches, the amount of ceramic is the most. When the ratio is increased, the amount of ceramic decreases, and the structure becomes softer, so the critical load parameters decrease. Since in a 1-8-1 sandwich, the amount of ceramic is lower than the 2-1-2 one, it is clear that the critical load parameter is lower. However, the results in sandwich type II are different, and in the 1-8-1 sandwich, the amount of ceramic is the most. By increasing the ratio in a constant thickness, the amount of ceramic increases, and the structure becomes stiffer, so the critical load parameters increase at lower gradient indices, especially in “N=0”. Since in 1-8-1 sandwich type-II, the amount of ceramic is more than 2-1-2, it is clear that the critical load parameter is higher. But from a certain value of the power law index, by increasing the ratio, the critical load of the 2-1-2 becomes more than 1-8-1 sandwiches. By increasing the power law index in a constant thickness, the ceramic quantity of the FG layer decreases, so, for all values of “hc/ht”, the critical load parameters decrease for both types of sandwiches. For sandwich type-I (S-S), in “hc/ht=0.5”, the critical load parameter decreases by 14.82% when “N” is increased, and in “hc/ht=8”, the critical load parameter decreases by 12.08% when “N” is increased. Also, for “N=0”, by increasing this ratio, the critical load decreases 19.89%, but for "N=2", it decreases 17.31%. For sandwich type-I (C-C), in “hc/ht=0.5”, the critical load parameter decreases by 21.74% when “N” is increased, and in “hc/ht=8”, the critical load parameter decrease 7.16% when “N” is increased. Also,

for “N=0”, by increasing this ratio, the critical load decreases by 16.89%, but for "N=2", it decreases by 1.41%. For sandwich type-II (S-S), in “hc/ht=0.5”, the critical load parameter decreases by 0.774% when “N” is increased, and in “hc/ht=8”, the critical load parameter decreases by 13.51% when “N” is increased. Also, for “N=0”, by increasing this ratio, the critical load increases by 8.83%, but for "N=2", it decreases by 5.13%. For sandwich type-II (C-C), in “hc/ht=0.5”, the critical load parameter decreases by 6.74% when “N” is increased, and in “hc/ht=8”, the critical load parameter decreases by 22.04% when “N” is increased. Also, for “N=0”, by increasing this ratio, the critical load increases by 26.23%, and for "N=2", it increases by 5.51%.

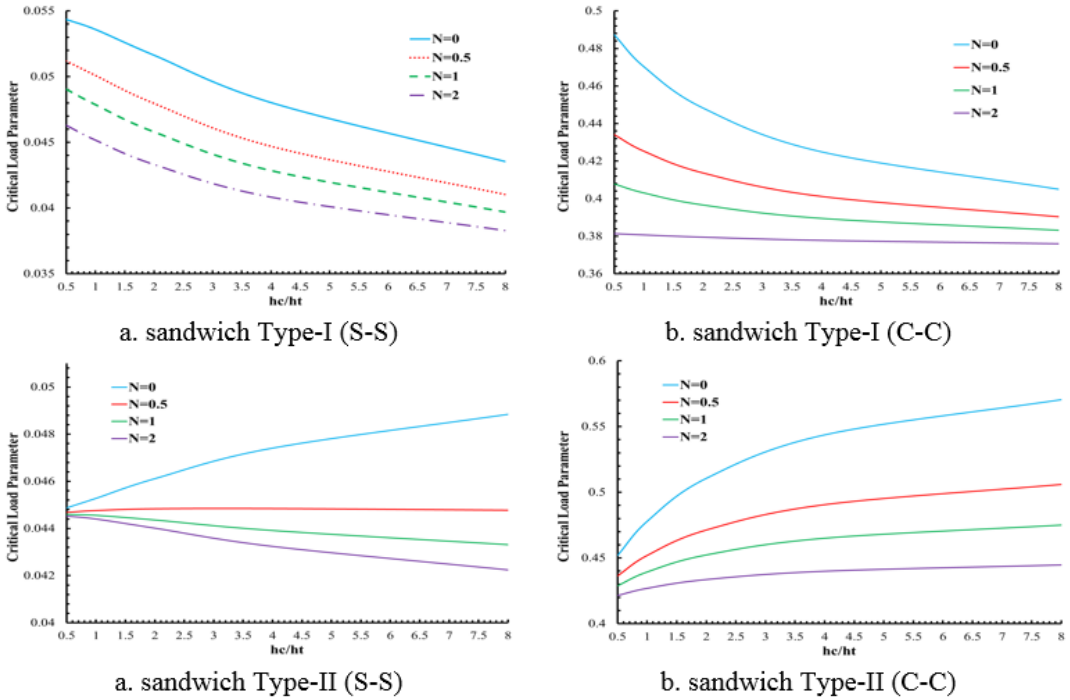

Figure 4. Critical load variation versus “hc/ht” ratio in different types of sandwich beams

The effect of the variation of the total thickness of the sandwiches, “h”, on the critical load parameter in various power law indices for different simply supported and clamped FG sandwich beams is depicted in Figure 5. Geometrical parameters are “T=300K, m=1, L/h=10”. It is obvious that by increasing the total thickness in a constant “L/h” ratio, the critical load parameter decreases. The slope of decreasing the critical load in the value of lower than 0.02 m is sever for all types of sandwiches, but in the higher values, the slope of decreasing reduces and in the (C-C) sandwich types is lower than (S-S) sandwich types. It means after a certain value, increasing the thickness has little effect on the critical load. For example, when “L/h=10” and “N=0”, by increasing the “h”, the critical load decreases 95.50% for sandwich type-I (S-S), 24.00% for (C-C) sandwich type-I, 95.64% for sandwich type-II (S-S) and 20.31% for sandwich type-II (C-C). However, it is seen that after the “h=0.02m”, the rate of variation is decreased for both sandwiches. For “h=0.01m”, by increasing “N”, the critical load parameter decreased by 11.29% for sandwich type I (S-S), 7.86% for sandwich type I (C-C), and 14.41% for sandwich type II (S-S) and 20.66% for sandwich type II (C-C).

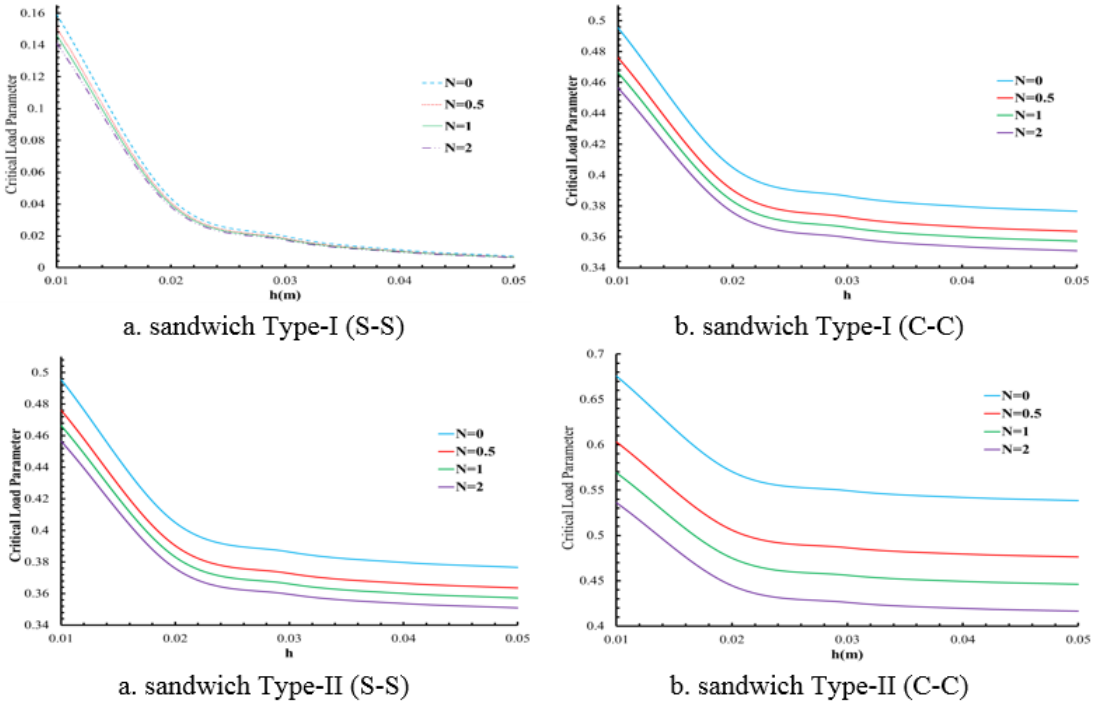

Figure 5. Critical load variation versus thickness in different types of sandwich beams

The effect of the variation of the wave number, "m", on the critical load parameters for various power law indices and constant total thickness is shown in Figure 6. Geometrical parameters are "h=0.02m, T=300K, m=1, L/h=10". It is clear that by increasing the wave number, the critical load parameters increase. In sandwich type-I (S-S) and sandwich type-II (S-S), in the lower wave numbers, the critical load parameters of both sandwiches are close to each other. Although in the lower wave numbers, the critical load of the (C-C) is too high than the (S-S) ones, in the higher wave numbers, the values of the critical load parameters in the case of (S-S) are close to (C-C). In sandwich type I (S-S), in "N=0", by increasing the wave number, the critical load parameter increase 1330.26% and, in sandwich type I (C-C), in "N=0", by increasing the wave number, the critical load parameter increase 101.137%, in sandwich type II (S-S), in "N=0", by increasing the wave number, the critical load parameter increase 1515.86% and, in sandwich type II (C-C), in "N=0", by increasing the wave number, the critical load parameter increase 90.98%.

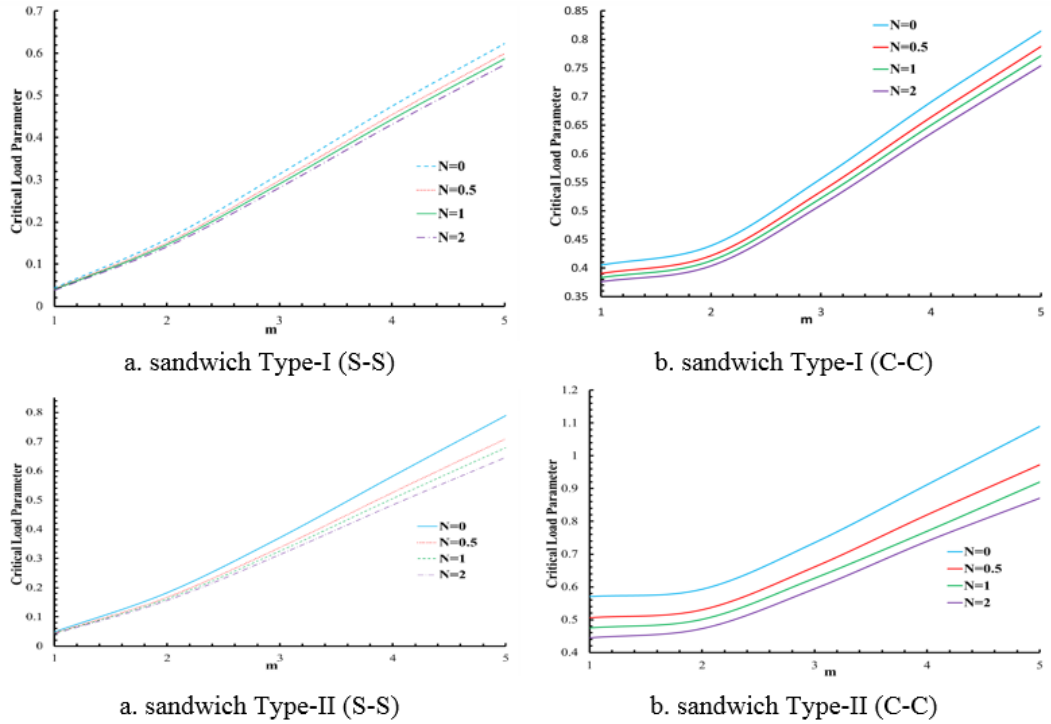

a. sandwich Type-I (S-S) b. sandwich Type-I (C-C)

a. sandwich Type-II (S-S) b. sandwich Type-II (C-C)

Figure 6. Critical load variation versus wave number in different types of sandwich beams

To clearly understand the porosity influence, Figures 7 and 8 show the effect of even and uneven porosity distributions on the critical load parameters of the different types of sandwich beams, respectively. As shown in these figures, in both types of sandwiches, by increasing the porosity volume fraction, the critical load parameter decreases. These decreases are stronger in the case of even porosity distribution in both sandwiches. In even distributions, porosities occur all over the cross-section of the FG layer. While, in uneven distribution, porosities are available at the middle zone of the cross-section. In sandwich type I (S-S), and for the even case and "N=0", by increasing the volume fraction of the porosity, the critical load decreases 26.31%, and in the uneven case in "N=0", by increasing the volume fraction of the porosity, the critical load decreases 13.45%. In sandwich type I (C-C), and for the even case and "N=0", by increasing the volume fraction of the porosity, the critical load decreases 10.01%, and in the uneven case in "N=0", by increasing the volume fraction of the porosity, the critical load decreases 4.87%. In sandwich type II (S-S), and for the even case and "N=0", by increasing the volume fraction of the porosity, the critical load decreases 22.67%, and in the uneven case in "N=0", by increasing the volume fraction of the porosity, the critical load decreases 6.00%. And, in sandwich type II (C-C), and for the even case and "N=0", by increasing the volume fraction of the porosity, the critical load decreases 28.45%, and in the uneven case in "N=0", by increasing the volume fraction of the porosity, the critical load decreases 13.32%.

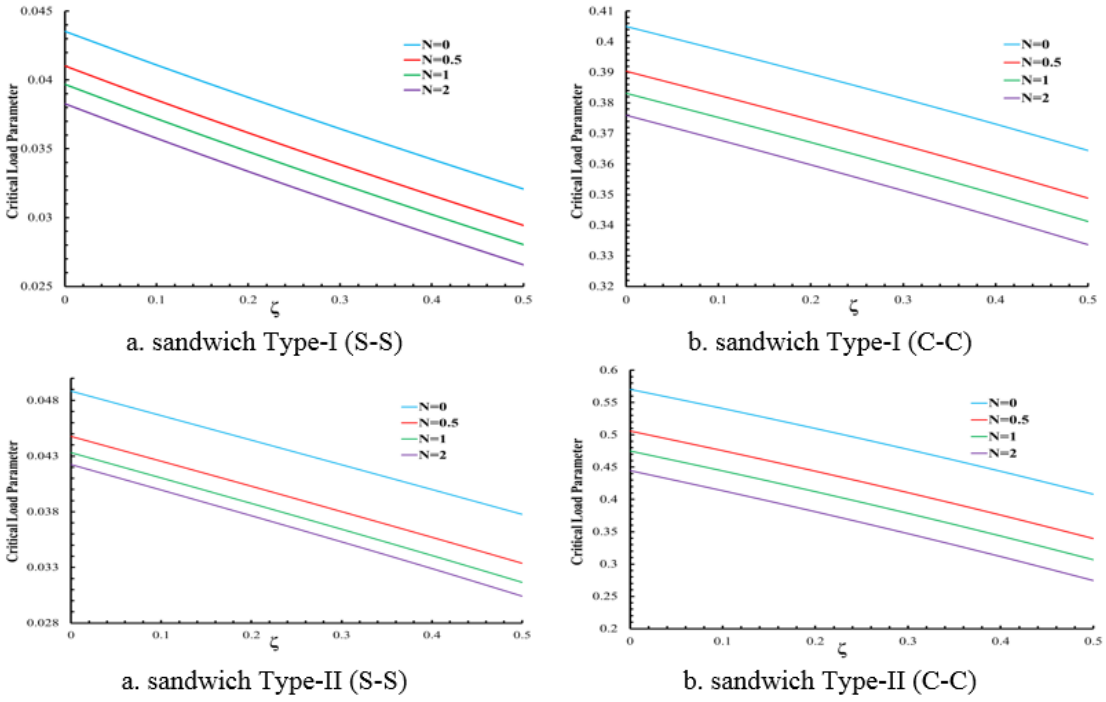

Figure 7. Critical load variation versus even porosity in different types of sandwich beams

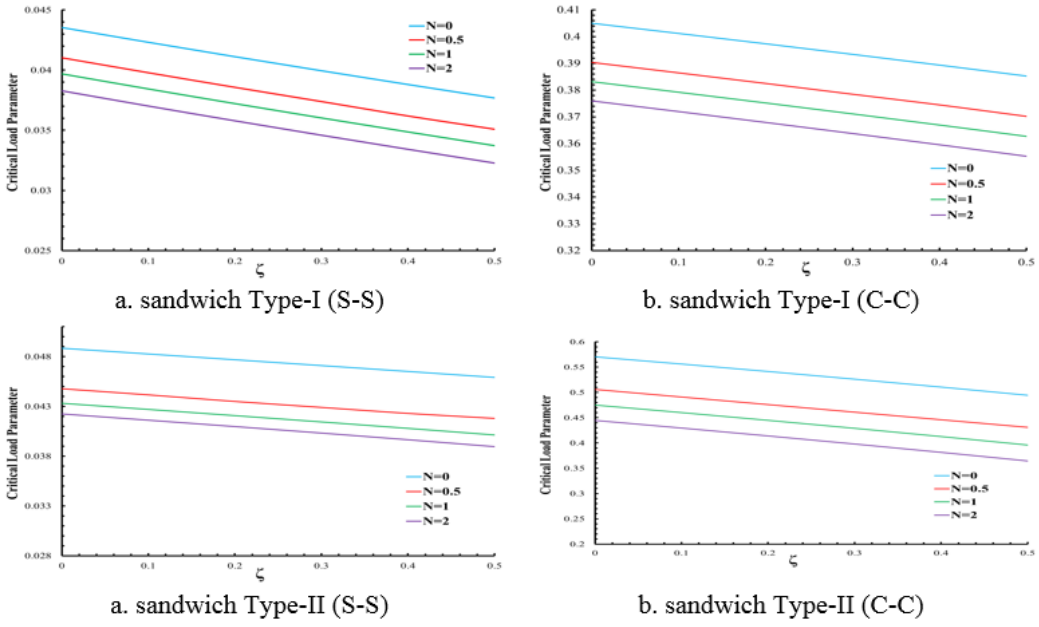

Figure 8. Critical load variation versus uneven porosity in different types of sandwich beams

4. Conclusion

By applying a modified high-order sandwich beam theory and considering the high-order stress resultants and thermal stress resultants, in-plane stresses and thermal stresses, and nonlinear strains in face-sheets and core, the buckling behavior of two types of porous FG sandwich beams which were temperature-dependent was investigated in this paper. The displacement fields of the face sheets and the core were considered based on the first-order shear deformation theory and the polynomial distributions, respectively. A power law distribution modified by considering even and uneven porosity distributions was used to model the material properties of the FG layers. The FG layers were

location dependent too. The governing equations were obtained by the minimum potential energy principle and solved by using the Galerkin method for simply supported and clamped boundary conditions. Also, a method was applied to reduce the number of the equations. Effects of temperature, thickness, and length, wave number, and porosities distributions on the critical load were discussed. The following conclusion can be drawn:

- By increasing the temperature, the critical load parameters decrease. In sandwich type-I (S-S), when "N=0", by increasing the temperature, the critical load parameter decreases 85.00%, for "N=1" and "N=2" it decreases 97.77%, and 97.44%, respectively. In sandwich type-I (C-C), when "N=0", by increasing the temperature, the critical load parameter decreases 60.51%, for "N=1" and "N=2" it decreases 68.03%, and 70.49%, respectively. And in sandwich type-II (S-S), when "N=0", by increasing the temperature, the critical load parameter decreases 90.10%, for "N=1" and "N=2" it decreases 81.15%, and 77.53%, respectively. And in sandwich type-II (C-C), when "N=0", by increasing the temperature, the critical load parameter decreases 33.03%, for "N=1" and "N=2" it decreases 49.78%, and 55.00%, respectively.
- The stability of sandwich type II is higher than type I in high-temperature conditions.
- By increasing the power law index, the critical load parameters decrease. For example, in sandwich type-I (S-S), sandwich type-I (C-C), sandwich type-II (S-S), and sandwich type-II (C-C) for "L/h=5", by increasing "N", the critical load parameter decrease 11.29, 7.86%, 14.41%, and 20.66%, respectively.
- The critical load parameters of the sandwiches with simply supported boundary conditions are lower than sandwiches with clamped (C-C) boundary conditions.
- The sandwich type-II with the clamped boundary condition is the most resistant sandwich in the high-temperature environments.
- By increasing the length-to-thickness ratio, the stability of the structure reduces, so the critical load parameter decreases.
- Variations of the core-to-face-sheet thickness ratio have different effect on sandwiches. In type-I by increasing the ratio, the critical load parameters decrease, but in type-II, first the critical load parameters increase at lower gradient indices, and from a certain value of the power law index, by increasing the power law index, when the ratio is increased, the critical load parameters decrease. For sandwich type-I (S-S), sandwich type-I (C-C), sandwich type-II (S-S), and sandwich type-II (C-C), in "hc/ht=0.5", the critical load parameter decreases by 14.82%, 21.74%, 0.774% and 6.74% when "N" is increased, and in "hc/ht=8", the critical load parameter decrease 12.08%, 7.16%, 13.51%, and 22.04%, respectively, when "N" is increased.
- By increasing the thickness in a constant L/h ratio, the critical load parameters decrease.
- By increasing the wave number, the critical load parameter increases.
- By increasing the porosity volume fraction in both even and uneven distributions, the critical load parameters decrease. Also, the variation of critical load in even porosity cases is more than uneven cases.

5. References

[1] Rahmani, M., Mohammadi, Y. and Kakavand, F. 2019. Vibration analysis of sandwich truncated conical shells with porous fg face sheets in various thermal surroundings. Steel and Composite Structures. 32(2): 239-252. doi:10.12989/scs.2019.32.2.239.

[2] Rahmani, M., Mohammadi, Y., Kakavand, F. and Raeisifard, H. 2020. Vibration analysis of different types of porous fg conical sandwich shells in various thermal surroundings. Journal of Applied and Computational Mechanics. 6(3): 416-432. doi:10.22055/jacm.2019.29442.1598.

[3] Frostig, Y., Baruch, M., Vilnay, O. and Sheinman, I. 1992. High-order theory for sandwich-beam behavior with transversely flexible core. Journal of Engineering Mechanics. 118(5): 1026-1043. doi:10.1061/(ASCE)0733-9399(1992)118:5(1026).

[4] Fazzolari, F.A. 2018. Generalized exponential, polynomial and trigonometric theories for vibration and stability analysis of porous fg sandwich beams resting on elastic foundations. Composites Part B: Engineering. 136: 254-271. doi:10.1016/j.compositesb.2017.10.022.

[5] Wu, H., Kitipornchai, S. and Yang, J. 2015. Free vibration and buckling analysis of sandwich beams with functionally graded carbon nanotube-reinforced composite face sheets. International Journal of Structural Stability and Dynamics. 15(07): 1540011. doi:10.1142/S0219455415400118.

[6] Li, Y., Dong, Y., Qin, Y. and Lv, H. 2018. Nonlinear forced vibration and stability of an axially moving viscoelastic sandwich beam. International Journal of Mechanical Sciences. 138: 131-145. doi:10.1016/j.ijmecsci.2018.01.041.

[7] Nguyen, T.-K., Vo, T.P., Nguyen, B.-D. and Lee, J. 2016. An analytical solution for buckling and vibration analysis of functionally graded sandwich beams using a quasi-3d shear deformation theory. Composite Structures. 156: 238-252. doi:10.1016/j.compstruct.2015.11.074.

[8] Kahya, V. and Turan, M. 2018. Vibration and stability analysis of functionally graded sandwich beams by a multi-layer finite element. Composites Part B: Engineering. 146: 198-212. doi:10.1016/j.compositesb.2018.04.011.

[9] Tossapanon, P. and Wattanasakulpong, N. 2016. Stability and free vibration of functionally graded sandwich beams resting on two-parameter elastic foundation. Composite Structures. 142: 215-225. doi:10.1016/j.compstruct.2016.01.085.

[10] Nguyen, T.-K., Nguyen, T.T.-P., Vo, T.P. and Thai, H.-T. 2015. Vibration and buckling analysis of functionally graded sandwich beams by a new higher-order shear deformation theory. Composites Part B: Engineering. 76: 273-285. doi:10.1016/j.compositesb.2015.02.032.

[11] Vo, T.P., Thai, H.-T., Nguyen, T.-K., Inam, F. and Lee, J. 2015. A quasi-3d theory for vibration and buckling of functionally graded sandwich beams. Composite Structures. 119: 1-12. doi:10.1016/j.compstruct.2014.08.006.

[12] Challamel, N. and Girhammar, U.A. 2011. Variationally-based theories for buckling of partial composite beam–columns including shear and axial effects. Engineering structures. 33(8): 2297-2319. doi:10.1016/j.engstruct.2011.04.004.

[13] Bhangale, R.K. and Ganesan, N. 2006. Thermoelastic buckling and vibration behavior of a functionally graded sandwich beam with constrained viscoelastic core. Journal of Sound and Vibration. 295(1-2): 294-316. doi:10.1016/j.jsv.2006.01.026.

[14] Hamed, M.A., Mohamed, S.A. and Eltaher, M.A. 2020. Buckling analysis of sandwich beam rested on elastic foundation and subjected to varying axial in-plane loads. Steel and Composite Structures. 34(1): 75-89. DOI: doi:10.12989/scs.2020.34.1.075.

[15] Li, C., Shen, H.-S. and Wang, H. 2019. Thermal post-buckling of sandwich beams with functionally graded negative poisson's ratio honeycomb core. International Journal of Mechanical Sciences. 152: 289-297. doi:10.1016/j.ijmecsci.2019.01.002.

[16] Liu, Y., Su, S., Huang, H. and Liang, Y. 2019. Thermal-mechanical coupling buckling analysis of porous functionally graded sandwich beams based on physical neutral plane. Composites Part B: Engineering. 168: 236-242. doi:10.1016/j.compositesb.2018.12.063.

[17] Paul, A. and Das, D. 2017. A study on non-linear post-buckling behavior of tapered timoshenko beam made of functionally graded material under in-plane thermal loadings. The Journal of Strain Analysis for Engineering Design. 52(1): 45-56. doi:10.1177/0309324716671857.

[18] Yin, Z., Gao, H. and Lin, G. 2021. An efficient semi-analytical static and free vibration analysis of laminated and sandwich beams based on linear elasticity theory. The Journal of Strain Analysis for Engineering Design.): 03093247211062688. doi:10.1177/03093247211062688.

[19] Askari, M., Brusa, E. and Delprete, C. 2021. On the vibration analysis of coupled transverse and shear piezoelectric functionally graded porous beams with higher-order theories. The Journal of Strain Analysis for Engineering Design. 56(1): 29-49. doi:10.1177/0309324720922085

[20] Fouda, N., El-Midany, T. and Sadoun, A. 2017. Bending, buckling and vibration of a functionally graded porous beam using finite elements. Journal of applied and computational mechanics. 3(4): 274-282. doi:10.22055/jacm.2017.21924.1121

[21] Gao, C. F., Pan, Y.-H., Zhang, W., Rao, J. X. and Huang, Y. 2021. Buckling of two-directional functionally graded cylindrical beams based on a high-order cylindrical beam model. International Journal of Structural Stability and Dynamics. 21(7): 2150099. doi:10.1142/S0219455421500991

[22] Basaglia, C. and Camotim, D. 2015. Buckling analysis of thin-walled steel structural systems using generalized beam theory (gbt). International Journal of Structural Stability and Dynamics. 15(1):1540004. doi:10.1142/S0219455415400040

[23] Akbaş, Ş.D. 2015. On post-buckling behavior of edge cracked functionally graded beams under axial loads. International Journal of Structural Stability and Dynamics. 15(4):1450065. doi:10.1142/S0219455414500655

[24] Grygorowicz, M., Magnucki, K. and Malinowski, M. 2015. Elastic buckling of a sandwich beam with variable mechanical properties of the core. Thin-Walled Structures. 87: 127-132. doi:10.1016/j.tws.2014.11.014

[25] Ellali, M., Bouazza, M. and Amara, K. 2022. Thermal buckling of a sandwich beam attached with piezoelectric layers via the shear deformation theory. Archive of Applied Mechanics. 92(3): 657-665. doi:10.1007/s00419-021-02094-x

[26] Nejati, M., Jafari, S.S., Dimitri, R. and Tornabene, F. 2022. Thermal buckling and vibration analysis of sma hybrid composite sandwich beams. Applied Sciences. 12(18): 9323. doi:10.3390/app12189323

[27] Chai, Y., Li, F. and Zhang, C. 2022. A new method for suppressing nonlinear flutter and thermal buckling of composite lattice sandwich beams. Acta Mechanica. 233:121–136. doi:10.1007/s00707-021-03107-0

[28] Safaei, B., Onyibo, E.C. and Hurdoganoglu, D. 2022. Thermal buckling and bending analyses of carbon foam beams sandwiched by composite faces under axial compression. Facta Universitatis, Series: Mechanical Engineering. 20(3): 589-615. doi:10.22190/FUME220404027S

[29] Mesmoudi, S., Askour, O., Rammane, M., Bourihane, O., Tri, A. and Braikat, B. 2022. Spectral chebyshev method coupled with a high order continuation for nonlinear bending and buckling analysis of functionally graded sandwich beams. International Journal for Numerical Methods in Engineering. 123(24): 6111-6126. doi:10.1002/nme.7105.

[30] Eltaher, M.A. and Mohamed, S.A. 2020. Buckling and stability analysis of sandwich beams subjected to varying axial loads. Steel and Composite Structures, An International Journal. 34(2): 241-260. doi:10.12989/scs.2020.34.2.241

[31] Liu, J., He, B., Ye, W. and Yang, F. 2021. High performance model for buckling of functionally graded sandwich beams using a new semi-analytical method. Composite Structures. 262: 113614. doi:10.1016/j.compstruct.2021.113614

[32] Belarbi, M. O., Garg, A., Houari, M. S. A., Hirane, H., Tounsi, A. and Chalak, H. 2021. A three-unknown refined shear beam element model for buckling analysis of functionally graded curved sandwich beams. Engineering with Computers. 38: 273–4300 1-28. doi:10.1007/s00366-021-01452-

[33] Waddar, S., Pitchaimani, J., Doddamani, M. and Barbero, E. 2019. Buckling and vibration behaviour of syntactic foam core sandwich beam with natural fiber composite facings under axial compressive loads. Composites Part B: Engineering. 175: 107133. doi:10.1016/j.compositesb.2019.107133

[34] Rahmani, M., Mohammadi, Y. and Kakavand, F. 2020. Buckling analysis of different types of porous fg conical sandwich shells in various thermal surroundings. Journal of the Brazilian Society of Mechanical Sciences and Engineering. 42(4): 1-16. doi:10.1007/s40430-020-2200-2

[35] Rahmani, M., Mohammadi, Y., Kakavand, F. and Raeisifard, H. 2019. Buckling behavior analysis of truncated conical sandwich panel with porous fg core in different thermal conditions. Amirkabir Journal of Mechanical Engineering. 52(10): 141-150. doi: 10.22060/mej.2019.15966.6240.

[36] Rahmani, M. and Dehghanpour, S. 2020. Temperature-dependent vibration of various types of sandwich beams with porous fgm layers. International Journal of Structural Stability and Dynamics. 21(2): 2150016. doi:10.1142/S0219455421500164

[37] Kheirikhah, M., Khalili, S. and Fard, K.M. 2012. Biaxial buckling analysis of soft-core composite sandwich plates using improved high-order theory. European Journal of Mechanics-A/Solids. 31(1): 54-66. doi:10.1016/j.euromechsol.2011.07.003

[38] Rahmani, M. and Mohammadi, Y. 2021. Vibration of two types of porous fg sandwich conical shell with different boundary conditions. Structural Engineering and Mechanics. 79(4): 401-413. doi:10.12989/sem.2021.79.4.401

[39] Vo, T.P., Thai, H. T., Nguyen, T. K., Maheri, A. and Lee, J. 2014. Finite element model for vibration and buckling of functionally graded sandwich beams based on a refined shear deformation theory. Engineering structures. 64: 12-22. doi:10.1016/j.engstruct.2014.01.029

[40] Reddy, J.N. 2003. Mechanics of Laminated Composite Plates and Shells: Theory and Analysis, Second Edition. CRC Press.